Journal of Applied Polymer Science

Ferroelectric Nanodot Formation from Spin-Coated Poly(vinylidene fluoride-*co*-trifluoroethylene) Films and Their Application to Organic Solar Cells

Yoon-Young Choi,[1]* Kyungwon Kwak,[2]* Ji-Won Seo,[3] Moonkyu Park,[1] Haemin Paik,[1] Jung-Yong Lee,[3] Jongin Hong,[2] Kwangsoo No[1]

[1]Department of Materials Science and Engineering, KAIST, Daejeon 305-701, Korea
[2]Department of Chemistry, Chung-Ang University, Seoul 156-756, Korea
[3]Graduate School of EEWS, KAIST Institute for the Nano Century, KAIST, Daejeon 305-701, Korea
*Yoon-Young Choi and Kyungwon Kwak equally contributed to this article
Correspondence to: J. Hong (E-mail: hongj@cau.ac.kr) and K. No (E-mail: ksno@kaist.ac.kr)

ABSTRACT: We demonstrated a facile route to the preparation of self-assembled poly(vinylidene fluoride-*co*-trifluoroethylene) [P(VDF-TrFE)] nanodots from spin-coated thin films. We found that the initial film thickness would play an important role in the formation of such P(VDF-TrFE) nanodots. Interestingly, the electric dipoles of such nanodots were self-aligned toward the bottom electrode and their ferroelectric properties were determined by using piezoresponse force microscopy. In addition, the self-polarized ferroelectric nanostructures were introduced to small molecular organic photovoltaic devices and allowed for enhancing the short circuit current density (J_{sc}) from 9.4 mA/cm^2 to 10.2 mA/cm^2 and the power conversion efficiency from 2.37% to 2.65%. © 2014 Wiley Periodicals, Inc. J. Appl. Polym. Sci. **2014**, *132*, 41230.

KEYWORDS: coatings; films; morphology; surfaces and interfaces

Received 6 December 2013; accepted 26 June 2014
DOI: 10.1002/app.41230

INTRODUCTION

Organic ferroelectric materials have been highly desirable in potential applications, such as non-volatile memories, radio-frequency identification (RFID) tags, and piezoelectric energy harvesters.[1–4] It is however only recent that the incorporation of a ferroelectric polymer interlayer into organic solar cells (OSCs) was demonstrated for enhancing the power conversion efficiency (PCE) due to the electric field induced by ferroelectric dipoles.[5] Among various organic ferroelectric materials, poly(vinylidene fluoride-*co*-trifluoroethylene), P(VDF-TrFE), copolymers are fascinating ones in contrast with ferroelectric oxides because of their large remnant polarization, short switching time, and the low processing temperature.[6–8] A considerable amount of efforts have been made to date in an attempt to improve the ferroelectric properties of P(VDF-TrFE) ultrathin films and nanostructures.[9–15] Solution spin-coating has commonly been used to prepare P(VDF-TrFE) ultrathin films even if several parameters, such as the initial polymer concentration, residual solvent, spin speed, and annealing temperature, affect the quality of their films.[9–12] P(VDF-TrFE) ultrathin films with an excellent crystalline order, on the other hand, have been achieved using a Langmuir–Blodgett (LB) monolayer (ML) transfer technique.[13] Spontaneous crystalline nanomesa formation from continuous P(VDF-TrFE) LB films has also been reported.[14] However, the LB ML transfer technique is sensitive to surface chemistry associated with the P(VDF-TrFE) coverage on water surface prior to its transfer. Additionally, in terms of self-organizing nanostructures, 8 ML and thicker films were unable to form discrete nanostructures even after lengthy post-annealing.[15] We accordingly investigated the self-organization of nanostructures from continuous spin-coated P(VDF-TrFE) films. Their ferroelectric properties were also evaluated involving piezoresponse force microscopy (PFM) and local piezoresponse hysteresis measurements. It should be noted that the movement of the main carbon backbone during the self-organization was determined using polarization controlled Fourier transform infrared spectroscopy (FTIR). We moreover demonstrated the enhancement of PCE in small molecular OSCs by the incorporation of self-polarized ferroelectric nanostructures to the cells.

Additional Supporting Information may be found in the online version of this article.

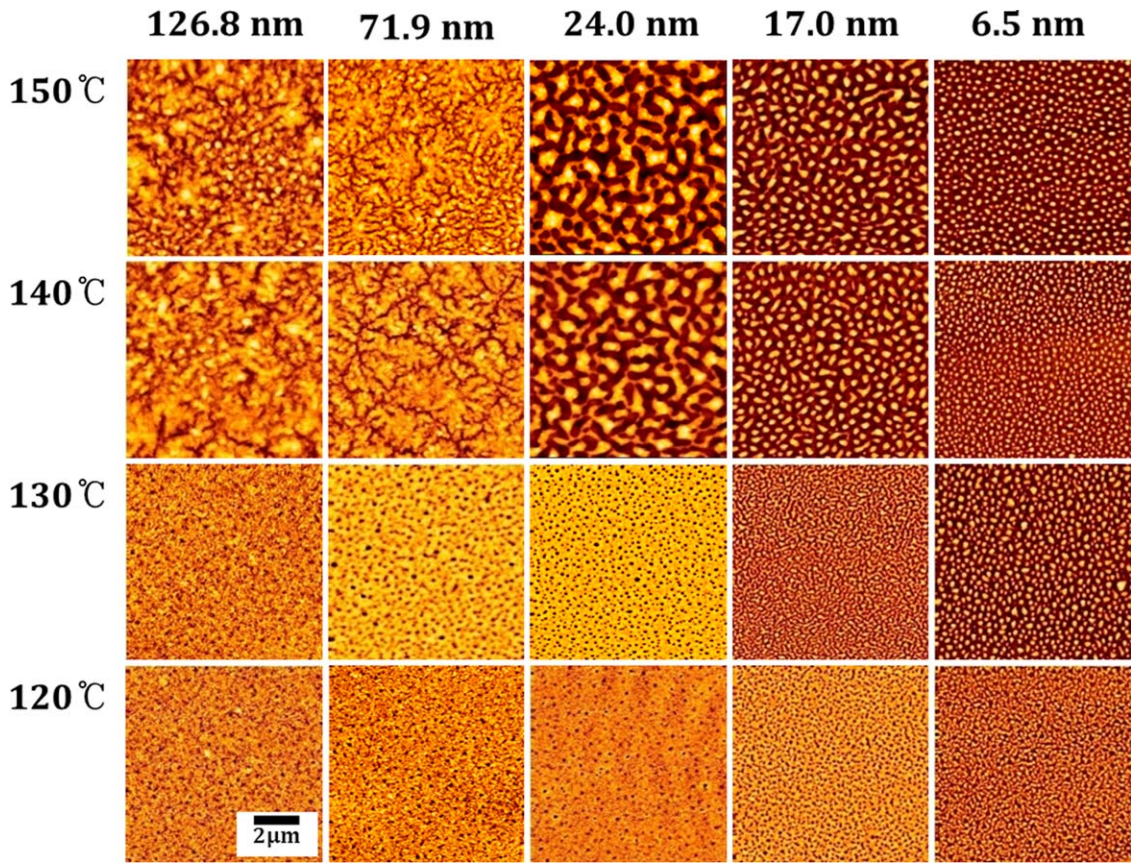

Figure 1. AFM images of P(VDF-TrFE) films annealed at 150°C: initial thicknesses of (a) 126.8 ± 7.1 nm, (b) 71.9 ± 3.2 nm, (c) 24.03 ± 3.5 nm, (d) 17.02 ± 0.11 nm, and (e) 6.48 ± 0.13 nm. [Color figure can be viewed in the online issue, which is available at wileyonlinelibrary.com.]

EXPERIMENTAL

In this study, self-organized P(VDF-TrFE) nanodots were obtained by spin-coating and subsequent annealing. We selected a ferroelectric copolymer consisting of 75% vinylidene fluoride and 25% trifluoroetylene (75 : 25 copolymer) with a molecular weight of 200,000 and its pellets were dissolved in methyl ethyl ketone (MEK) to prepare solutions with concentrations ranging from 0.25 wt % to 3 wt %. The solutions were filtered through a 0.2-μm syringe filter and then spun cast onto Au/Ti/Si substrates at 5000 rpm for 20 s. The spin-coated P(VDF-TrFE) films were then immediately annealed at a specific temperature for 2 h on a hot plate. The initial thickness of each spin-coated P(VDF-TrFE) film just after drying solvent was measured to discover a critical thickness of the self-assembled nanodot formation using a scanning electron microscope (S-4800, Hitachi, Japan), a transmission electron microscope (JEM-2100F HR, JEOL, Japan), and a spectroscopic ellipsometer (VASE, J.A. Woollam, USA). The surface morphology was observed using a commercial atomic force microscope (AFM, SPA 400, Seiko, Japan) with a SiN cantilever tip. In order to determine ferroelectric molecular conformations of P(VDF-TrFE) films and nanostructures, we utilized a FTIR spectrometer (Vertex 80, Bruker Optics, Germany) with an image microscope (Hyperion 3000, Bruker Optics, Germany). Importantly, the polarization of an incident light in the FTIR-attenuated total reflection (ATR) spectroscopy was controlled in an attempt to explore molecular orientations of P(VDF-TrFE) copolymers during the self-organization. Incident p-polarized light redefines the polarizing direction of an evanescent wave which penetrates into the sample and is used as a probe beam in FTIR-ATR measurements. The sampling area was around 80 × 80 μm^2 and the spectral

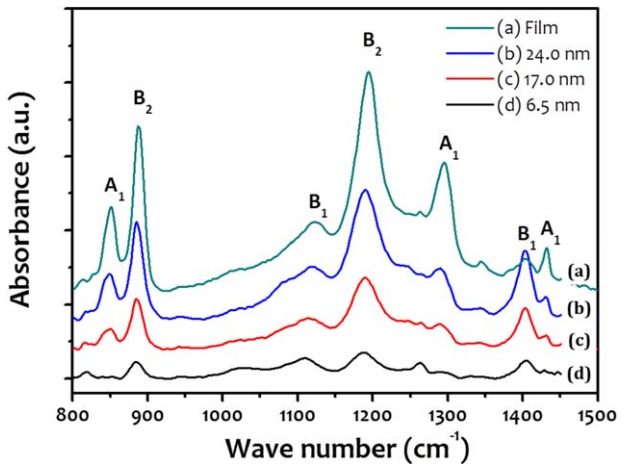

Figure 2. p-Polarized FTIR-ATR spectra of the P(VDF-TrFE) nanostructures obtained from (a) 24.03 ± 3.5 nm, (b) 17.02 ± 0.11 nm, and (c) 6.48 ± 0.13 nm-thick P(VDF-TrFE) films. [Color figure can be viewed in the online issue, which is available at wileyonlinelibrary.com.]

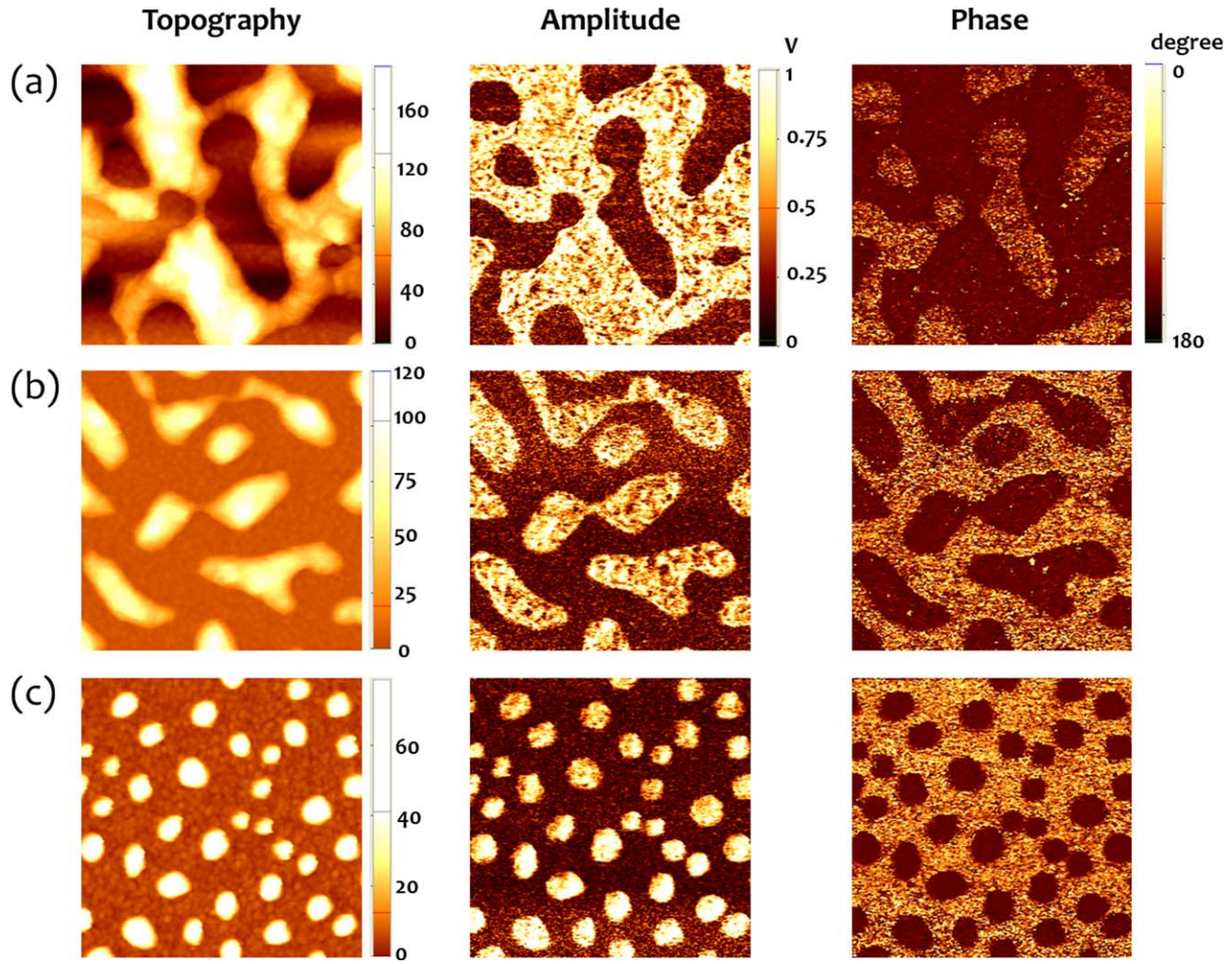

Figure 3. (a)Topological, (b) piezoelectric amplitude, and (c) phase images of the self-assembled P(VDF-TrFE) nanodots with initial film thicknesses of (top) 24.03 ± 3.5 nm, (middle) 17.02 ± 0.11 nm, and (bottom) 6.48 ± 0.13 nm. [Color figure can be viewed in the online issue, which is available at wileyonlinelibrary.com.]

resolution was 4 cm^{-1}. Both morphological and piezoresponse images were simultaneously recorded, under ambient conditions, using a commercial AFM (XE-100, Park Systems, Korea) equipped with a lock-in amplifier (SR830, Stanford Research System, USA). A controlled modulation voltage of 0.8 V_{rms} at 17 kHz was applied to a Pt-coated Si tip (Micromasch, Spring constant $k \approx 6.0$ N/m), which allowed the measurement of local electrical and topological properties both simultaneously and independently. Piezoelectric hysteresis loops of continuous films and self-organized nanostructures were measured by positioning the tip on top of a selected position and monitoring the piezoresponse signal as a function of the d.c. bias applied to the bottom electrode. We calibrated photodiode voltage outputs of the piezoelectric vibration using force-distance measurements to convert them to effective d_{33} piezoresponse (pm V^{-1}). In order to determine the efficacy of ferroelectric nanodots on the performance of OSCs, we also fabricated small molecular organic photovoltaic devices whose structure used in this study was Ag (100 nm)/bathocuprione (BCP, 8 nm)/fullerene (C_{60}, 20 nm)/copper phthalocyanine (CuPc):C60 (1 : 1, 30 nm)/P(VDF-TrFE) nanodots/indium tin oxide (ITO). CuPc and C60 co-evaporated on P(VDF-TrFE) nanodots formed on ITO : glass substrates and additional C60 was subsequently deposited. BCP and Ag layers, eventually, evaporated by the process of thermal evaporation. The photovoltaic characteristics of the devices under AM 1.5 global one sun illumination (100 mW/cm^2) were investigated by a solar cell *I–V* measurement system (K3000 LAB, McScience, Korea). Photocurrent density (J_{sc}), open-circuite voltage (V_{oc}), fill factor (FF), and power-conversion-efficiency (η) were simultaneously measured.

RESULTS AND DISCUSSION

Illustrated in Figure 1 is the effect of film thickness and annealing temperature on surface morphology. We observed that the formation temperature of the P(VDF-TrFE) nanodots decreased as the initial film thickness decreased. For example, the film with the initial thickness of 17.02 ± 0.11 nm (0.5 wt %) gradually changed from the continuous film to the isolated nanodots between 120 and 150°C. This progressive evolution indicated

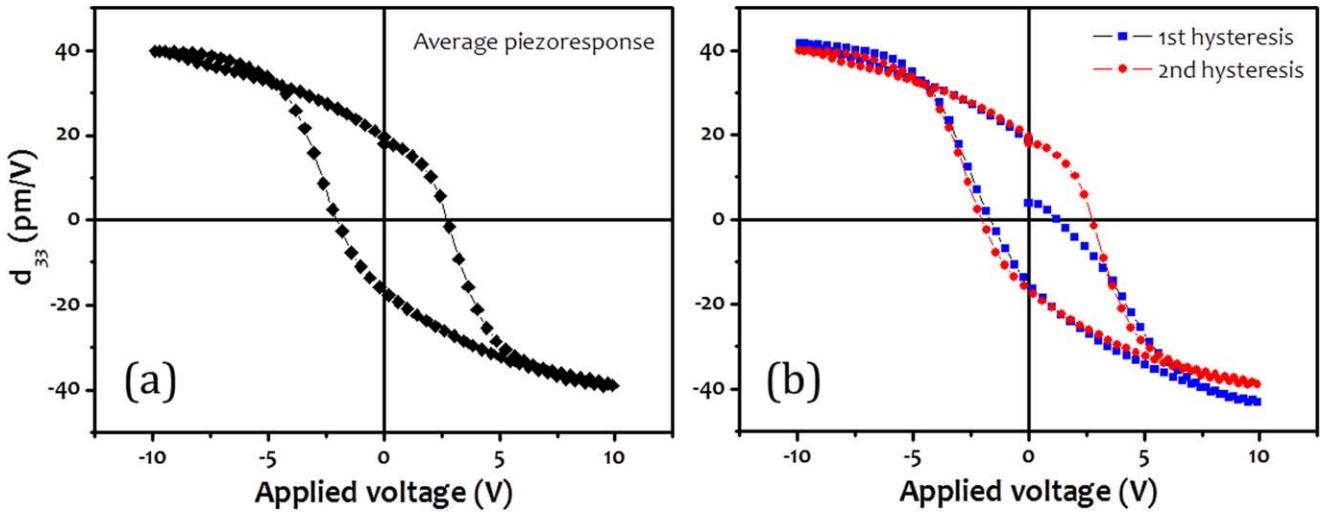

Figure 4. Piezoresponse hysteresis loops of P(VDF–TrFE) nanodots. [Color figure can be viewed in the online issue, which is available at wileyonlinelibrary.com.]

that the formation of P(VDF-TrFE) nanostructures would depend on the initial film thickness and that there was a critical thickness ($t < 24.03 \pm 3.5$ nm) at which nanostructures were formed. In cross-sectional TEM images, the shape of the discrete nanodots was hemispherical and they were clearly separated from one another on the substrate (Supporting Information Figure S1). It should be noted that 25-nm thick and thicker films would not be thermally changed to the discrete nanodots even after higher temperature is applied. We speculate that such critical thickness in spin-cast polymer films would be associated with the extent of polymer deformation related to the competition between shear-induced structuring and thermally activated interdiffusion.[16] However, the interdiffusion in the polymeric films in relation to the conformational restructuring during annealing process is restricted by the propagation of pinhole defects below the critical thickness.[16,17] Thus, in the regime below the critical thickness (called a sublayer), shear stresses associated with spin coating could stretch and/or disentangle P(VDF-TrFE) polymers. We, in addition, observed that the formation of nanostructures was affected by the substrate material, such as Al and Cu (Supporting Information Figure S2). The smaller nanodots were formed on the Al-coated Si substrate, whilst nanodots were not formed on the Cu-coated Si substrate. The surface roughness of the substrate would affect the formation of such nanodots (i.e., the break-up of polymer films into small droplets) and their feature size (Supporting Information Table S1). This might also be expected from the differences in thermal conductivity[18,19] and interface adhesion energies.[20,21]

The conformation characterization of the P(VDF-TrFE) film and nanostructures was investigated using the p-polarized FTIR-ATR spectroscopy. Figure 2 shows p-polarized FTIR-ATR spectra of P(VDF-TrFE) samples with different initial thicknesses annealed at 150°C. The absorption bands at 1290 cm^{-1} and 848 cm^{-1} (A_1, $\boldsymbol{\mu} \| \boldsymbol{b}$) are associated with the β-phase possessing *trans* sequences longer than four monomers ($t_m > 4$) and *trans* sequences longer than three monomers ($t_m > 3$), respectively.[22–24] It is notable that the 1293 cm^{-1} band can be used as a reference band when determining relative intensities within a sample since it does not overlap with any disordered-phase band. Those at 1195 cm^{-1} and 885 cm^{-1} (B_2, $\boldsymbol{\mu} \| \boldsymbol{a}$) are related to anti-symmetric CF_2 stretching vibrations and *trans* sequence of one monomer.[22–24] Those at 1402 $cm^{-1}$and 1076 cm^{-1} (B_1, $\boldsymbol{\mu} \| \boldsymbol{c}$) are very sensitive to the orientation of carbon main chains that can interact with the p-polarized light.[22–24] Unfortunately, the 1076 cm^{-1} band overlaps with broad disordered-phase bands and thus they cannot be used to evaluate the chain direction of films and nanostructures. We should note that the calculated penetration depth of our FTIR-ATR measurements is 650 nm and thus the penetration depth is enough to cover all samples used in this study, along with the fact that the absolute decrease of peak intensities with the decrease in the initial thickness is caused by smaller quantity of P(VDF-TrFE) copolymers. In Figure 2, absorption peaks parallel to an in-plane *a* axis and a vertical polar *b* axis decreased as the initial film thickness decreased (i.e., smaller nanodots were formed). The absorption peak parallel to the chain *c* axis, in contrast, prominently grows in isolated nanodots. This indicates that P(VDF-TrFE) copolymers start to be progressively aligned to the vertical direction when nanodots are being formed during the post-annealing process.

We think that the fundamental mechanism of self-organizing nanodots would be related to the mass transfer along an interface between two phases due to surface tension gradient or temperature gradient or both. In our case, MEK plays a key role in creating the temperature gradient due to its high volatility. The MEK evaporation can also cause a concentration variation within the films and this would result in the surface energy variation on the interface between the copolymers and the air. In addition, the hydrodynamic flow during spin coating stretches the polymer chains and thus they are predominantly parallel to the substrate. Xia et al. reported that P(VDF-TrFE) thin films exhibited the stronger peak at $\chi = 90°$ in the χ scan of the (110, 200) reflection than P(VDF-TrFE) thick films.[25] Park et al. also

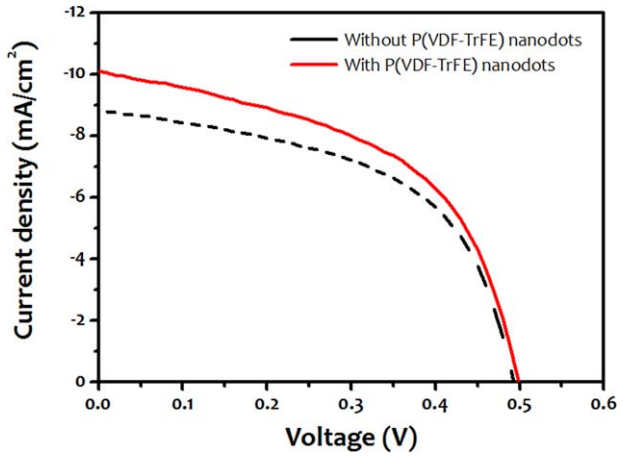

Figure 5. *J–V* characteristics of CuPc : C60 small-molecule OSCs with and without P(VDF-TrFE) nanodots. [Color figure can be viewed in the online issue, which is available at wileyonlinelibrary.com.]

confirmed that the strong bias centrifugal force field during spin coating resulted in the preferential alignment of molecular chains parallel to the substrate surface by the 2-dimensional grazing-incidence X-ray diffraction.[26] This coincides with the absorption peaks parallel to either *a* or *b* axis in our p-polarized FTIR-ATR spectroscopic analysis (Figure 2). The preferred orientation of P(VDF-TrFE) thin films used in this study was confirmed by the (110) peak at 20° (but not the (001) in-chain peak at 35°) in X-ray diffraction (Supporting Information Figure S3). During the self-organization, however, the surface of nanodots is being exposed to air and then polymer chains begin to be aligned perpendicular to the surface in order to increase the hydrophobic interaction with other polymers and reduce the hydrophilic interaction with the air. Such preferential alignment is to achieve the lowest total surface energy of the system. Thus, we anticipate that the absorption peak aligned perpendicular to the chain *c*-axis becomes the prominent one during the nanodot formation. This coincides with p-polarized FTIR results mentioned above.

Figure 3 shows topological, PFM amplitude, and PFM phase images of the P(VDF-TrFE) nanostructures. PFM imaging allows the understanding of the polarization distribution within individual nanostructures by detecting their mechanical oscillation in response to the applied ac bias (called piezoresponse). In the PFM measurements, an amplitude signal indicates the deviation of polarization from a surface normal (or a longitudinal piezoelectric coefficient), whilst a phase signal indicates the polarization direction. In our PFM phase images, bright contrast means upward polarization, whilst dark contrast means downward polarization. Interestingly, as-received P(VDF-TrFE) nanostructures showed uniform dark contrast in the phase images. It indicates that electric dipoles in the nanostructures were self-aligned in the direction from surface to the bottom electrode. To obtain more details about spatial arrangement of polarization, combined vertical and lateral PFM measurements can be carried out but this is beyond the scope of this study. In order to investigate switching properties of P(VDF-TrFE) nanodots (average diameter of 172.75 ± 40.5 nm and average height of 51.4 ± 10.6 nm), local piezoresponse hysteresis loops were measured at randomly selected positions and averaged data are shown in Figure 4(a). The P(VDF-TrFE) nanodots exhibited a remnant d_{33} value of 18.1 ± 3.3 pm/V comparable with the macroscopic values of 15–30 pm/V[27] and a coercive voltage of 2.4 ± 0.5 V. The hysteresis loop was positively shifted along the voltage axis. This hysteresis loop shift can be elucidated by the work function difference between top ($\Phi_{Pt} = 5.65$ eV) and bottom ($\Phi_{Au} = 5.1$ eV) electrodes and the polarization offset or non-switchable dipoles.[20] In addition, the percentage of the relative ratio for the aligned polarization per unit volume beneath the AFM tip can also be determined by comparing an initial d_{33} value from the firstly measured hysteresis loop with a remnant d_{33} value from the secondly measured hysteresis loop.[21] The relative portion of the self-polarization (i.e., a remnant polarization in the nanodots without any previous poling treatment) was 20.5% [Figure 4(b)]. Recently, we reported that such self-polarization in ferroelectric polymer films would be intimately linked with the built-in-voltage between the bottom electrode and the P(VDF-TrFE) layer due to Schottky barrier in the metal-semiconductor contact.[21] Furthermore, we investigated the effect of the annealing temperature (130, 150, and 170°C) on structural and ferroelectric switching properties of the nanodots (Supporting Information Figure S4 and Table S2). The absorption bands associated with the *β*-phase possessing *trans* sequences drastically decreased when 24-nm thick films were annealed at 170°C and thus the post-annealing above melting temperature (T_m) resulted in poor ferroelectric properties assessed by local piezoelectric hysteresis loops. Park et al. reported that the heat treatment above T_m led significant reduction of ferroelectric polarization in P(VDF-TrFE) thin films because of recrystallization.[26]

Table I. Photovoltaic Performance of CuPc:C_{60} OSCs Without and with Ferroelectric Nanodots

	V_{oc} (V)	J_{sc} (mA/cm^2)	FF (%)	PCE (%)
Without nanodots	0.49	−9.00	54	2.38
With nanodots	0.50	−10.10	52	2.64

Figure 5 illustrates the representative *J–V* characteristics of the OSCs with and without ferroelectric nanodots. The photovoltaic parameters are summarized in Table I. The addition of the self-polarized P(VDF-TrFE) nanodots between CuPc : C_{60} and ITO resulted in better photovoltaic performance: J_{sc} from 9.0 mA/cm^2 to 10.1 mA/cm^2, V_{oc} from 0.49 V to 0.50 V, and PCE from 2.38% to 2.64%. We think that the internal electric field induced by the self-polarized nanodots would affect the work function of the ITO electrode and thus the change in ITO work function would result in the improvement of Ohmic contact between CuPc : C_{60} and ITO related to hole transport from the active layer to anode. More details about their role in the OSCs are under investigation.

CONCLUSION

In conclusion, we have successfully fabricated P(VDF-TrFE) nanodots using the simple route of spin coating and

post-annealing. The self-assembly mechanism of such nanodots might involve the minimization of total surface energy. We found that the initial film thickness would play an important role in the formation of such P(VDF-TrFE) nanodots and that there was the critical initial film thickness, for example, $t < 24.0 \pm 3.5$ nm. The p-polarized FTIR-ATR spectroscopy confirmed P(VDF-TrFE) copolymers near the surface were aligned perpendicular to the interface when nanodots were formed during the post-annealing process. What drew our interest was that the insertion of the self-polarized nanodots between the active layer and the anode allowed for enhancing the photovoltaic parameters in the organic photovoltaic devices. We expect that the self-polarized nanodots offer a great promise in non-volatile memories, infrared imaging arrays, touch-screen sensors, and artificial skin applications. We are currently exploring the regulation of self-organizing nanostructures via external mechanism and the visualization of three dimensional dipole configuration in such nanodots using angle-resolved PFM (AR-PFM).[28]

ACKNOWLEDGMENTS

This research was supported by Basic Science Research Program (2013-026989) and Mid-career Research Program (2010-0015063, 2012-047815) through the National Research Foundation (NRF) of Korea funded by the Ministry of Science, ICT & Future Planning of Korea. K. Kwak acknowledges a financial support from NRF fund (No. 2009–0093817).

REFERENCES

1. Gelinck, G. H.; Marsman, A. W.; Touwslager, F. J.; Setayesh, S.; de Leeuw, D. M.; Naber, R. C. G.; Blom, P. W. M. *Appl. Phys. Lett.* **2005**, *87*, 092903.
2. Ling, Q. D.; Liaw D.-J., Zhu, C.; Chan, D. S.-H.; Kang, E.-T., Neoh, K.-G. *Prog. Polym. Sci.* **2008**, *33*, 917.
3. Taylor, G. W.; Burn, J. R.; Kammann, S. M.; Powers, W. B.; Welsh, T. R. *IEEE J. Oceanic Eng.* **2001**, *26*, 539.
4. Priya, S. *J. Electroceram.* **2007**, *19*, 165.
5. Yuan, Y.; Reece, T. J.; Sharma, P.; Poddar, S.; Durcharme, S.; Gruverman, A.; Yang, Y.; Huang, J. *Nat. Mater.* **2011**, *10*, 296.
6. Kochervinskii, V. V. *Crystallogr. Rep.* **2003**, *48*, 649.
7. Poulsen, M.; Durcharme, S. *IEEE Trans. Dielectric. Electric Insul.* **2010**, *17*, 1028.
8. Naber, R. C. G.; Asadi, K.; Blom, P. W. M.; de Leeuw, D. M.; de Boer, B. *Adv. Mater.* **2009**, *21*, 1.
9. Kang, S. J.; Park, Y. J.; Sung, J.; Jo, P. S.; Park, C.; Kim, K. J.; Cho, B. O. *Appl. Phys. Lett.* **2008**, *92*, 012921.
10. Ramasundaram, S.; Yoon, S.; Kim, K. J.; Lee, J. S.; Park, C. *Macromol. Chem. Phys.* **2009**, *210*, 951.
11. Choi, Y. Y.; Hong, J.; Leem, D.-S.; Park, M.; Song, H. W.; Sung, T.-H.; No, K. *J. Mater. Chem.* **2011**, *21*, 5057.
12. Park, M.; Choi, Y. Y.; Kim, J.; Hong, J.; Song, H. W.; Sung, T.-H.; No, K. *Soft Matter* **2012**, *8*, 1064.
13. Bune, A. V.; Fridkin, V. M.; Durcharme, S.; Blinov, L. M.; Palto, S. P.; Sorokin, A. V.; Yudin, S. G.; Zlatkin, A. *Nature* **1998**, *391*, 874.
14. Bai, M.; Durcharme, S. *Appl. Phys. Lett.* **2004**, *85*, 3528.
15. Li, J.; Luo, Y.; Bal, M.; Ducharme, S. *Appl. Phys. Lett.* **2005**, *87*, 213116.
16. Sills, S.; Overney, R. M. *J. Chem. Phys.* **2004**, *120*, 5334.
17. Wang, C. L.; Wang, S. *J. Phys. Rev. B* **1995**, *51*, 8810.
18. Ristenpart, W. D.; Kim, P. G.; Domingues, C.; Wan, J.; Stone, H. A. *Phys. Rev. Lett.* **2007**, *99*, 234502.
19. Gambaryan-Roisman, T. *Int. J. Heat Mass Transfer* **2010**, *53*, 390.
20. Reiter, G.; Sommer, J. U. *Phys. Rev. Lett.* **1998**, *80*, 3771.
21. Frank, C. W.; Rao, V.; Despotopoulou, M. M.; Pease, R. F. W.; Hinsber, W. D.; Miller, R. D.; Rabolt, J. F. *Science* **1996**, *273*, 912.
22. Kim, K. J.; Reynolds, N. M.; Hsu, S. L. *Macromolecules* **1989**, *22*, 4395.
23. Kim, K. J.; Hsu, S. L. *Polymer* **1994**, *35*, 3612.
24. Xu, H.; Shanthi, G.; Bharti, V.; Zhang, Q. *Macromolecules* **2000**, *33*, 4125.
25. Xia, F.; Razavi, B.; Xu, H.; Cheng, Z. Y.; Zhang, Q. M. *J. Appl. Phys.* **2002**, *92*, 3111.
26. Park, Y. J.; Kang, S. J.; Park, C.; Kim, K. J.; Lee, M. S.; Chung, U.-I.; Park, I. *J. Appl. Phys. Lett.* **2006**, *88*, 242908.
27. Omote, K.; Ohigashi, H.; Koga, K. *J. Appl. Phys.* **1997**, *81*, 2760.
28. Park, M.; Hong, S.; Kim, J.; Hong, J.; No, K. *Appl. Phys. Lett.* **2011**, *99*, 142909.